J. Phys. B: At. Mol. Opt. Phys. **21** (1988) 2117-2128. Printed in the UK

Electron impact ionisation of nickel ions

L J Wang†, K Rinn‡ and D C Gregory

Physics Division, Oak Ridge National Laboratory, Oak Ridge, Tennessee 37831-6372, USA

Received 26 January 1988

Abstract. Absolute cross section measurements at energies from below threshold to 1500 eV are reported for electron impact ionisation of nickel ions with initial charges 5+, 6+, 7+, 8+, 12+ and 14+. The experimental data are compared with distorted-wave calculations for direct ionisation, which account for 40–80% of the measured peak total ionisation cross sections. The discrepancy is attributed to contributions to single ionisation due to excitation of inner-subshell electrons followed by autoionisation. Ionisation rate coefficients and fitting parameters based on the data are presented for charge states 5+ through 8+.

1. Introduction

Electron impact ionisation is an important atomic process in both laboratory and astrophysical plasmas. Modelling studies of power balance, temperatures, equilibrium charge states and the interpretation of diagnostic information from injected impurities all depend in part on an accurate database of rate coefficients for electron impact excitation, ionisation and recombination (Palumbo 1971, Barnett 1983, Isler 1984). Accurate cross section measurements for electron impact ionisation of multiply charged ions are therefore necessary to provide such a database (Isler *et al* 1977) and to serve as benchmarks for comparison with detailed calculations in order to establish general scaling laws.

Nickel is an important impurity element in modern fusion research devices, especially in those where the vessel walls are constructed largely of high-nickel-content alloys (e.g., JET, the Joint European Torus). Knowledge of atomic processes involving nickel ions is essential in order to understand and accurately model these plasmas. However, the only crossed-beams measurements previously available are for ionisation of singly (Montague and Harrison 1985) and triply (Gregory and Howald 1986) ionised nickel. Detailed calculations which include indirect ionisation effects are also available only for charge states up to 3+ (Pindzola *et al* 1985, Burke *et al* 1987). The present measurements, in conjunction with calculations and measurements of the electron impact ionisation cross sections for a sequence of iron ions (Montague *et al* 1984, Mueller *et al* 1985, Gregory *et al* 1986, Gregory *et al* 1987), also provide the basis for testing scaling laws along isonuclear and isoelectronic sequences.

† On assignment from Wesleyan University, Middletown, Connecticut 06457, USA. Present address, Department of Physics and Astronomy, Vanderbilt University, Nashville, Tennessee 37235, USA.

‡ Joint research appointment with the Joint Institute for Laboratory Astrophysics, Boulder, Colorado 80309-0440, USA.

0953-4075/88/112117+12$02.50

Electron impact ionisation can be a rather complex process. A target ion may ionise through direct ionisation:

$$e + X^{q+} \rightarrow X^{(q+1)} + 2e \tag{1}$$

through excitation of an inner-subshell target electron followed by autoionisation:

$$e + X^{q+} \rightarrow (X^{q+})^{**} + e \rightarrow X^{(q+1)+} + 2e \tag{2}$$

or through more exotic processes such as resonant-excitation-double-autoionisation:

$$e + X^{q+} \rightarrow (X^{(q-1)+})^{**} \rightarrow X^{(q+1)+} + 2e. \tag{3}$$

The relative importance of each process changes along isoelectronic (same number of electrons) and isonuclear (same element) sequences. In general, indirect ionisation, dominated by process (2) above, has been found to become relatively more important as the ionic charge and the nuclear charge increase. This is demonstrated by the present measurements as well as in previous ionisation studies.

We report here the measured absolute cross sections of single ionisation for Ni^{5+}, Ni^{6+}, Ni^{7+}, Ni^{8+}, Ni^{12+} and Ni^{14+} by electron impact. The apparatus and details of the measurements are briefly described in the experimental section, followed by presentation and discussion of the results. Calculations of rate coefficients based on the data, along with fits to these calculations, are then described. Finally, we present our summary and conclusions.

2. Experimental

The detailed description of the experimental apparatus used in these experiments can be found elsewhere (Gregory *et al* 1986). A brief account of the experimental arrangement is given here.

For electron and ion beams crossing at 90°, the absolute cross section $\sigma(E)$ at an interaction energy E is determined by

$$\sigma(E) = \frac{Rqe^2}{I_i I_e} \frac{v_i v_e}{(v_i^2 + v_e^2)^{1/2}} \frac{F}{D} \tag{4}$$

where R is the signal event rate, q is the charge on the incident ion, e is the charge on an electron, v_i and v_e are the ion and electron velocities, I_i and I_e are the ion and electron currents and D is the detection efficiency. F is the form factor defined by

$$F = \frac{\int I_i(z)\,dz \int I_e(z)\,dz}{\int I_i(z)\, I_e(z)\,dz} \tag{5}$$

where z is the spatial coordinate perpendicular to both the electron and ion beams. The spatial beam profiles $I_i(z)$ and $I_e(z)$ are measured in the interaction volume with a precision probe driven by a stepping motor. The form factor can be determined to within 2%, and is typically between 4 and 5 mm. The detection efficiency D takes into account the incomplete transmission of signal ions to the detector, the detection efficiency of the electron multiplier and the pulse transmission of the electronics. The typical value of D is 0.95.

The nickel ions were extracted from the ORNL-ECR ion source, where they were generated from a piece of Inconel foil inserted into the magnetically confined source plasma. The details of the design and the performance of the ORNL-ECR ion source have been published by Meyer (1985).

The extracted ions were accelerated by 10 kV, analysed for the desired ratio of charge to mass, and transported to the ultrahigh-vacuum chamber shown in figure 1. The ion beam was directed into a 90° electrostatic analyser (labelled 'purifier' in figure 1) to remove any ions which changed charge during the flight from the ion source to this chamber. The ion and electron beams crossed at 90° in the interaction volume at the centre of the electron gun. The ion beam was then analysed by a double-focusing magnetic analyser to separate the further-ionised signal ions from the primary ion beam. The signal ions were counted in an electron multiplier, and the primary ions were collected in one of two Faraday cups, depending on the ratio of the primary to product ion charge. Typical values for the critical experimental parameters are listed for each target ion in table 1.

The electron gun is almost identical to that described by Taylor *et al* (1974). The electron beam is confined by a 25 mT axial magnetic field, which makes the beam density more uniform and its physical size at the collision volume almost independent of energy. The gun is designed to minimise spiralling of beam electrons and the escape of backscattered or secondary electrons from the collector. The electron beam is

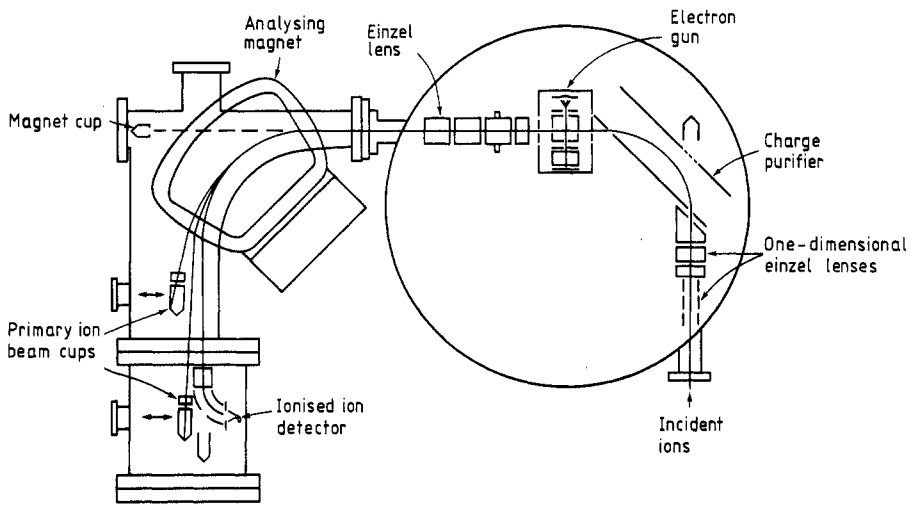

Figure 1. Schematic diagram of the crossed-beams collision chamber and post-collision magnetic charge analyser.

Table 1. Typical experimental parameters.

Parameter	Ni^{5+}	Ni^{6+}	Ni^{7+}	Ni^{8+}	Ni^{12+}	Ni^{14+}
Electron energy (eV)	300	400	500	600	1000	1300
Electron current (mA)	1.9	2.9	4.0	6.0	9.6	12.9
Ion current (particle nA)	2.3	2.4	1.0	1.8	3.2	0.2
Background count rate (Hz)	75	30	37	43	157	11.6
Signal count rate (Hz)	147	119	49	76	34	1.8

electronically chopped at a 50% duty cycle so that the background events occurring while the electron beam is off can be subtracted from events counted while the electron gun is on, and the net signal of electron impact ionisation can be determined. The energy spread in the electron beam is less than 2 eV (based on an extrapolation from Belic *et al* 1981).

3. Results

The measured cross sections for electron impact ionisation of Ni^{5+}, Ni^{6+}, Ni^{7+}, Ni^{8+}, Ni^{12+} and Ni^{14+} are tabulated in table 2 with relative uncertainties which combine statistical uncertainties at the one standard deviation level with fluctuations in the form factor. The statistical standard deviation is typically 1-5% of the peak cross section, and the uncertainty in the form factor measurement is normally 2% or less. Systematic uncertainties, which affect the overall magnitude of the cross section curves but not their shapes, are about 10% at the 90% confidence level. Previous publications (Crandall and Phaneuf 1978, Gregory *et al* 1986) discuss the error analysis in detail.

The cross section data are compared in the figures with distorted-wave calculations for direct ionisation by Buie and Pindzola (1987) utilising computer codes described by Pindzola *et al* (1983). These calculations are within 20% of results from the semiempirical one-parameter formula by Lotz (1968). Threshold energies for ionisation of the subshells that are predicted to contribute to single ionisation for each of these ions are listed in table 3. These configuration-average energies were calculated using the relativistically corrected Hartree-Fock atomic structure code by Cowan (1981).

3.1. Ni^{5+}, Ni^{6+}, Ni^{7+} and Ni^{8+}

The measured cross sections for Ni^{5+}, Ni^{6+}, Ni^{7+} and Ni^{8+} are plotted in figures 2-5. Relative uncertainties are shown in the figures where they are larger than the plotted points (in figure 4, typical relative uncertainties are shown). The shapes of these four cross section curves are similar, as are their ground-electron configurations ($3p^63d^n$, where $n = 5, 4, 3, 2$ with increasing charge). The measurements may be compared in the figures with distorted-wave calculations for direct ionisation from the 3s, 3p and 3d subshells. The direct ionisation of an electron from 2p or inner levels is predicted to result in a net double-ionisation event, and is therefore not considered for these cases. It appears from the calculations that direct ionisation accounts for about 80% of the peak experimental total cross section for Ni^{5+}, 75% for Ni^{6+} and 65% for Ni^{7+} and Ni^{8+}. The excitation of inner-subshell 2p, 3s and 3p electrons to autoionising levels is expected to be mainly responsible for the differences between the experimental and direct ionisation cross sections, with hundreds of level-to-level transitions contributing over the entire energy range studied. Preliminary detailed calculations for Ni^{8+} (Pindzola and Griffin 1987) which include excitation-autoionisation effects from these subshells are in good agreement with the measurements.

Recent R-matrix calculations by Burke *et al* (1987) considered the effects on total ionisation of six 3p-3d transitions to autoionising states in nickel ions. They concluded that these transitions would not affect ionisation of ions with initial charges of five and higher because the excited states become bound and cannot autoionise. However, it is clear from the present measurements that significant excitation-autoionisation occurs for more highly charged ions and that numerous additional transitions must be considered in order to obtain an accurate prediction of the total cross section.

Table 2. Experimental cross sections (in 10^{-18} cm^2) for ionisation of nickel ions. Relative uncertainties are quoted at the statistical one standard deviation level or equivalent.

Energy (eV)	Ni^{5+}	Ni^{6+}	Ni^{7+}	Ni^{8+}	Ni^{12+}	Ni^{14+}
91.6	0.064 ± 0.144					
96.1	0.255 ± 0.123					
100.8	0.491 ± 0.157					
103.2	0.90 ± 0.20					
105.8	1.67 ± 0.13					
108.2	2.68 ± 0.22					
110.5	3.32 ± 0.14					
113.0	4.59 ± 0.18					
115.6	5.26 ± 0.16					
116.1		−0.099 ± 0.158				
120.8		−0.096 ± 0.125				
125.5	6.96 ± 0.15	−0.043 ± 0.134				
130.8		0.500 ± 0.102				
133.2		1.24 ± 0.15				
135.5	8.23 ± 0.13	1.28 ± 0.11		0.04 ± 0.19		
140.4		2.56 ± 0.10				
145.1	9.40 ± 0.12	3.23 ± 0.15	0.03 ± 0.22	0.12 ± 0.10		
155.0	10.15 ± 0.12	4.35 ± 0.17	0.14 ± 0.20	0.09 ± 0.14		
159.7			0.37 ± 0.27			
164.7		5.21 ± 0.14	0.51 ± 0.21	0.15 ± 0.11		
169.9			1.38 ± 0.25			
174.7	11.86 ± 0.10	5.98 ± 0.13	1.86 ± 0.20	0.24 ± 0.12		
174.7			2.49 ± 0.22			
179.4			2.75 ± 0.20			
184.5			3.11 ± 0.14	0.19 ± 0.13		
194.5	12.86 ± 0.11	7.14 ± 0.13	3.93 ± 0.13	0.26 ± 0.13		
199.5				0.74 ± 0.12		
204.3			4.58 ± 0.20	1.37 ± 0.13		
209.2				1.58 ± 0.12		
213.7	13.64 ± 0.15					
214.3			5.10 ± 0.13	1.78 ± 0.12		
219.2		8.16 ± 0.16				
224.0				2.22 ± 0.11		
233.7	14.51 ± 0.13		5.69 ± 0.14	2.67 ± 0.12		
243.6		9.13 ± 0.13		3.13 ± 0.12		
252.9	15.22 ± 0.13		6.02 ± 0.13	3.13 ± 0.09		
263.1				3.54 ± 0.14		
268.1		9.70 ± 0.17				
272.7	15.29 ± 0.12		6.50 ± 0.13	3.61 ± 0.12		
292.6	15.29 ± 0.10	10.04 ± 0.12	6.43 ± 0.26	3.71 ± 0.13		
303.3					−0.023 ± 0.038	
316.9	15.13 ± 0.15		6.82 ± 0.11	4.01 ± 0.15		
327.5					0.025 ± 0.038	
342.2	15.29 ± 0.14	9.92 ± 0.09	6.81 ± 0.15	4.24 ± 0.14		
352.2					0.101 ± 0.029	
366.7	15.08 ± 0.15		6.87 ± 0.11	4.37 ± 0.13		
371.7					0.058 ± 0.028	
391.1	15.19 ± 0.13	9.84 ± 0.13	6.78 ± 0.09	4.38 ± 0.10	0.072 ± 0.029	
410.8					0.206 ± 0.050	
415.7			7.17 ± 0.13	4.59 ± 0.08		
431.0					0.327 ± 0.037	
440	15.03 ± 0.16	9.87 ± 0.13	6.98 ± 0.13	4.43 ± 0.10	0.014 ± 0.033	

Table 2. (continued)

Energy (eV)	Ni^{5+}	Ni^{6+}	Ni^{7+}	Ni^{8+}	Ni^{12+}	Ni^{14+}
451					0.427 ± 0.040	
465			7.16 ± 0.15	4.61 ± 0.11		
470					0.404 ± 0.040	
490	15.26 ± 0.08	9.89 ± 0.10	7.12 ± 0.13	4.52 ± 0.12	0.465 ± 0.053	0.129 ± 0.035
515					0.536 ± 0.039	
539	14.87 ± 0.11	9.82 ± 0.07	7.06 ± 0.13	4.45 ± 0.11	0.538 ± 0.036	
564					0.605 ± 0.034	
589	14.52 ± 0.14	9.58 ± 0.07	7.07 ± 0.12	4.44 ± 0.11	0.656 ± 0.032	0.238 ± 0.029
637	14.30 ± 0.12	9.58 ± 0.06	7.09 ± 0.11	4.58 ± 0.10	0.638 ± 0.032	
688	14.21 ± 0.27	9.44 ± 0.06	6.92 ± 0.10	4.57 ± 0.09	0.674 ± 0.040	0.275 ± 0.024
736	14.65 ± 0.14	9.69 ± 0.08	7.07 ± 0.09	4.51 ± 0.11	0.680 ± 0.034	
787	14.13 ± 0.15	9.43 ± 0.08	6.98 ± 0.13	4.44 ± 0.09	0.747 ± 0.028	0.319 ± 0.023
787		9.77 ± 0.12				
812						0.306 ± 0.019
837			6.99 ± 0.08	4.50 ± 0.11	0.734 ± 0.032	0.261 ± 0.015
860					0.813 ± 0.029	0.331 ± 0.018
885	13.14 ± 0.14	9.42 ± 0.08	6.66 ± 0.13	4.69 ± 0.15	0.877 ± 0.031	0.403 ± 0.019
910					0.946 ± 0.028	0.443 ± 0.033
934			6.48 ± 0.13	4.62 ± 0.11	0.971 ± 0.029	0.508 ± 0.019
959					0.928 ± 0.037	
985	12.90 ± 0.15	8.90 ± 0.18	6.58 ± 0.12	4.41 ± 0.12	0.912 ± 0.023	0.532 ± 0.019
1034					0.994 ± 0.023	0.621 ± 0.024
1083		8.41 ± 0.06	6.21 ± 0.11	4.17 ± 0.15	0.940 ± 0.021	0.604 ± 0.046
1131	11.55 ± 0.13					0.587 ± 0.048
1183		8.07 ± 0.06	5.94 ± 0.10	4.03 ± 0.16	0.961 ± 0.028	0.582 ± 0.043
1279	10.64 ± 0.11				0.940 ± 0.028	0.586 ± 0.033
1327		7.35 ± 0.07	5.43 ± 0.11	3.83 ± 0.06		
1379					0.881 ± 0.020	0.514 ± 0.035
1478	9.40 ± 0.13	6.81 ± 0.05	5.13 ± 0.08	3.71 ± 0.08	0.898 ± 0.021	

Table 3. Threshold energies for ionisation of subshells of nickel ions. These configuration-average energies (in eV) are calculated using the relativistic Hartree–Fock code by Cowan (1981).

Ion	Subshell	Energy	Subshell	Energy	Subshell	Energy
Ni^{5+} ($3s^23p^63d^5$)	$3d^5$	103.8	$3p^6$	173.5	$3s^2$	221.1
Ni^{6+} ($3s^23p^63d^4$)	$3d^4$	131.3	$3p^6$	200.1	$3s^2$	248.5
Ni^{7+} ($3s^23p^63d^3$)	$3d^3$	160.0	$3p^6$	227.6	$3s^2$	277.1
Ni^{8+} ($3s^23p^63d^2$)	$3d^2$	191.2	$3p^6$	257.4	$3s^2$	307.2
Ni^{12+} ($3s^23p^4$)	$3p^4$	387.9	$3s^2$	433.8		
Ni^{14+} ($3s^23p^2$)	$3p^2$	459.1	$3s^2$	499.4		

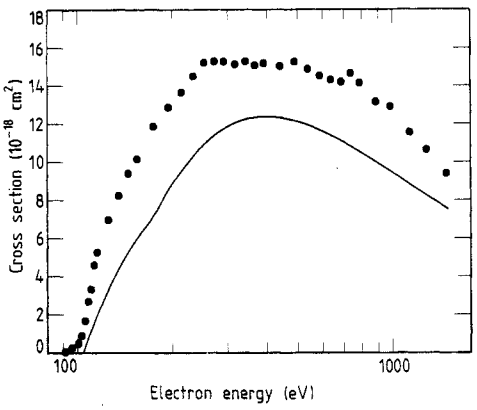

Figure 2. Electron impact ionisation cross sections for $e + Ni^{5+} \rightarrow Ni^{6+} + 2e$. Full circles are the present data; relative uncertainties at the one standard deviation level are smaller than the plotted points. The curve is a distorted-wave calculation for direct ionisation by Buie and Pindzola (1987).

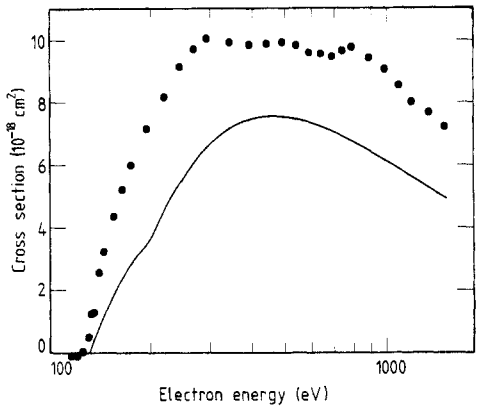

Figure 3. Electron impact ionisation cross section for $e + Ni^{6+} \rightarrow Ni^{7+} + 2e$. Notation is the same as for figure 2.

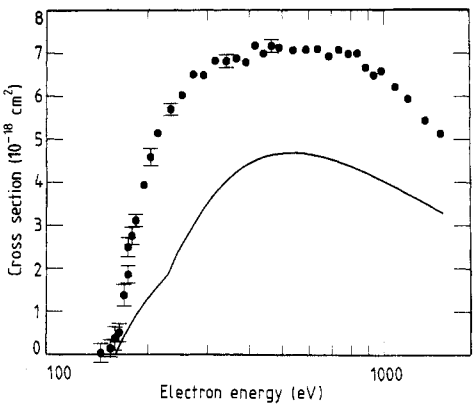

Figure 4. Electron impact ionisation cross section for $e + Ni^{7+} \rightarrow Ni^{8+} + 2e$. Full circles are the present measurements; typical relative uncertainties are shown at the one standard deviation level. The curve is a distorted-wave calculation for direct ionisation by Buie and Pindzola (1987).

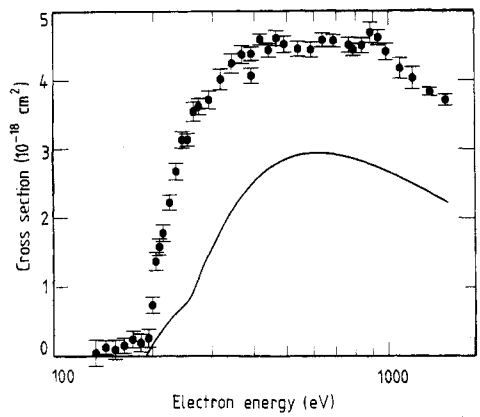

Figure 5. Electron impact ionisation cross section for $e + Ni^{8+} \rightarrow Ni^{9+} + 2e$. Full circles are the present measurements; relative uncertainties are plotted at the one standard deviation level. The curve is a distorted-wave calculation for direct ionisation by Buie and Pindzola (1987).

A variation of the Lotz formula has been proposed by Burgess and Chidichimo (1983) for use along with a scheme of modified inner-subshell ionisation potentials which accounts for excitation-autoionisation. The procedure is expected to work best in those cases where excitation-autoionisation contributes to the cross section from threshold and no single transition dominates the indirect contribution. In those cases which meet these criteria, a smooth featureless enhancement of the ionisation cross section may be expected. The Burgess-Chidichimo procedure simulates this enhancement near threshold by lowering the effective ionisation potential of the inner electrons. At high energies, however, this artificial enhancement disappears as the effects of lower

ionisation thresholds dwindle. This behaviour is, in fact, observed in comparing the present data with the predictions of the Burgess-Chidichimo procedure. For Ni^{5+}, agreement with the experimental results is excellent up to 450 eV; the calculation underestimates the cross section at higher energies. At 1500 eV, the Burgess-Chidichimo predictions approach the distorted-wave direct calculations and are only 8% higher. A similar pattern is observed for Ni^{6+}, while the Burgess-Chidichimo results underestimate the indirect contributions at all energies for Ni^{7+} and Ni^{8+}. The procedure is, however, an improvement over direct ionisation calculations at near-threshold energies for favourable cases such as those described here.

The present results may also be compared with recent measurements and detailed calculations (Gregory *et al* 1986, Pindzola *et al* 1986) for the isoelectronic iron ions (Fe^{3+}-Fe^{6+}). For those ions, it was found that indirect ionisation is significant, accounting for 30-50% of the total cross sections. However, the indirect ionisation contributions were found to depend on the precise levels populated by the excited electrons and on which of these excited levels are above the ionisation limit. It is, in general, very difficult to accurately predict the effects of excitation transitions with thresholds very near the ionisation threshold.

The observed thresholds for ionisation of Ni^{5+}, Ni^{6+} and Ni^{7+} are consistent with those expected for ground-configuration ion beams. However, we do observe a significant cross section below the threshold for ionisation of ground-state Ni^{8+}. This is a signature for the existence of ions in metastable states in the projectile beam. Based on the observed threshold, and assuming that the cross section for ionisation of the metastable ion is similar in magnitude and energy dependence to that of the ground-state ion, we estimate that about 10% of the Ni^{8+} ion beam was in the metastable $3p^63d4s$ configuration. No metastable component was observed in ionisation of the isoelectronic iron ion Fe^{6+}.

The above four ions have a number of features in common. Indirect ionisation is observed near the threshold and continues to make a significant contribution to the highest energies measured here. In comparison with the calculated direct ionisation predictions, excitation-autoionisation becomes proportionally more important as the ion charge increases for these ions. No sharp features are observed which would indicate that a single isolated transition dominates the excitation-autoionisation component of the cross section. Apparently, numerous transitions to autoionising levels contribute to a seemingly smooth indirect ionisation contribution.

3.2. *Ni^{12+} and Ni^{14+}*

The electron impact ionisation cross sections for Ni^{12+} and Ni^{14+} are plotted in figures 6 and 7, respectively. Relative uncertainties at the one standard deviation level are plotted for each point. Two major differences are observed between these cross section curves and those of the group discussed above. First, distorted-wave calculations of direct ionisation accounts for most of the observed cross section at the lower energies (e.g., over 80% of the experimental total cross section below 800 eV for Ni^{12+}), in contrast to the trend noted above that indirect processes play a more important role as the ion charge increases. Second, the onset of indirect ionisation is clearly observed for both Ni^{12+} and Ni^{14+} as a distinct rise in cross section beginning at an electron energy of about 850 eV. Based on calculations for the isoelectronic iron ion (Pindzola *et al* 1987), we suggest that the sudden increase in cross section is mainly due to the excitation of 2p electrons to the 3p and 3d subshells followed by autoionisation.

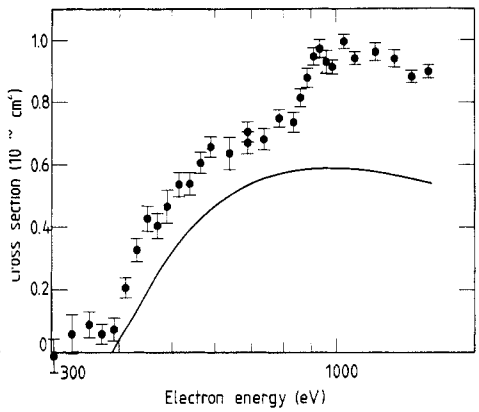

Figure 6. Electron impact ionisation cross section for $e + Ni^{12+} \rightarrow Ni^{13+} + 2e$. Notation is the same as for figure 5.

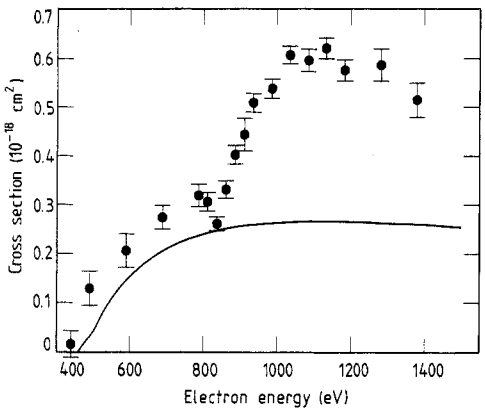

Figure 7. Electron impact ionisation cross section for $e + Ni^{14+} \rightarrow Ni^{15+} + 2e$. Notation is the same as for figure 5.

Although the 2p-3p and 2p-3d excitations leave the ion in a highly excited state with sufficient energy to double autoionise, the fraction which undergoes a single ionisation event should be dominant.

Although the indirect ionisation cross sections in Ni^{12+} and Ni^{14+} are small compared with those for lower charge states, excitation-autoionisation involving $\Delta n = 1$ transitions is significant. In this and a number of other cases (e.g., Pindzola *et al* 1987), indirect ionisation remains almost constant while the direct ionisation decreases with increasing charge, so that excitation-autoionisation due to a specific transition becomes relatively more important with increasing ionic charge until the excited state no longer autoionises. A similar trend was noted by Burke *et al* (1987), but was interpreted from a different viewpoint. Indirect ionisation contributions due to $\Delta n = 1$ transitions were predicted by them to be negligible, based on calculations for lower charge states of nickel.

Predictions based on the Burgess-Chidichimo formula were also compared with the present data. For these two ions, with a strong enhancement of the cross section well above the ionisation threshold dominated by a few transitions, this procedure does not significantly improve on direct ionisation calculations.

A dip is observed in the cross section for Ni^{14+} between 800 and 830 eV. This feature was found to be reproducible within the stated uncertainties. We have no satisfactory physical explanation for it except to suggest that it may be due to interference effects connected with the onset of 2p-3p excitation.

A non-zero cross section is observed for Ni^{12+} below the threshold energy for direct ionisation, indicating that the ion beam includes some ions in metastable states (probably with a $3p^3 3d$ configuration). Assuming that the cross sections are the same for ionisation of ground-state and metastable ions, we estimate that approximately half of the Ni^{12+} ion beam was in a metastable configuration.

4. Rate coefficients

Data on ionisation are often useful to many users (e.g., plasma modellers) in the form of rate coefficients. A computer program has been developed by the Controlled Fusion

Atomic Data Center at Oak Ridge National Laboratory for the conversion of cross sections to rate coefficients and to provide covenient fits to the resulting rate coefficient curves. The methods of calculation (see the section on Gaussian quadrature in Mathews and Walker 1970) and fitting (Gregory *et al* 1986) will not be discussed here.

In order to provide an adequate basis for convolution with Maxwellian electron energy distributions, cross sections are required over a larger range of energies than could be measured. For Ni^{5+}-Ni^{8+}, the trends of the highest-energy measurements were extrapolated with a logarithmic function which blended into the direct ionisation calculations at energies between 4 and 6 keV. The values from theory were then used for cross sections up to 10^5 eV. The rate coefficients at selected energies for Ni^{5+}-Ni^{8+} are listed in table 4. It should be noted that the high temperature ($1000 < kT < 3000$) rate coefficients in table 4 may vary by 15% depending on the adopted extrapolation procedure. The present measurements for Ni^{12+} and Ni^{14+} do not extend to sufficiently high energies to establish the asymptotic energy dependence of the cross section. Instead of attempting to blindly extrapolate the data to high energies, we have chosen not to predict rate coefficients for these two ions.

Table 4. Ionisation rate coefficients for Ni^{5+}-Ni^{8+}. The rate coefficients (in units of 10^{-10} cm^3 s^{-1}) at selected values of kT (in eV) were derived from the present data.

kT (eV)	Ni^{5+}	Ni^{6+}	Ni^{7+}	Ni^{8+}
10	0.0036	0.0002		
20	0.6614	0.1193	0.0224	0.0044
30	3.987	1.155	0.3584	0.1001
40	10.07	3.684	1.455	0.4977
70	34.97	17.13	9.068	4.130
100	59.49	32.52	19.19	9.795
150	92.37	54.79	35.08	19.66
200	116.6	72.00	48.00	28.30
300	148.0	95.69	66.25	41.27
400	166.0	110.5	77.66	50.00
700	185.0	130.3	92.11	63.72
1000	185.3	134.7	94.51	69.36
2000	168.8	125.7	86.03	70.34
3000	154.0	113.5	77.09	65.53

In order to provide an accurate fit to the rate coefficients, which span several decades in both temperature and α, the natural logarithms of the rate coefficients listed in table 4 have been fitted to a Chebyshev polynomial expansion (Abramowitz and Stegun 1970) following the method reported by Cox and Hayes (1973). The fitting coefficients a_n ($n = 0, 1, \ldots, 8$) are listed in table 5 and may be used to calculate the rate coefficient at any value of kT between 10 and 3000 eV. The expansion may be accomplished through a direct expansion of Chebyshev polynomials of the first kind by the formula

$$\alpha(kT) = \exp\left(\tfrac{1}{2}a_0 + \sum_{r=1}^{8} a_r T_r(x)\right) \tag{6}$$

where the rate coefficient α is in cm^3 s^{-1}, kT is in eV and the reduced energy x is given by

$$x = \ln[(kT)^2/E_{\min}E_{\max}]/\ln(E_{\max}/E_{\min}) \tag{7}$$

Table 5. Rate coefficient fitting parameters. E_{min} and E_{max}, which set the range of validity of the fit and are used in the calculation of the reduced energy x [see equation (7)], are 10 and 3000 eV, respectively. Fitting parameters a_0-a_8 are used in equation (6) to calculate ionisation rate coefficients for these ions.

Ion	a_0	a_1	a_2	a_3	a_4	a_5	a_6	a_7	a_8
Ni^{5+}	−41.120	4.3948	−2.4542	0.840 81	−0.282 72	0.087 87	−0.014 53	0.001 44	−0.002 37
Ni^{6+}	−43.148	5.5332	−3.0631	1.104 0	−0.382 58	0.103 06	−0.017 78	0.004 86	−0.001 70
Ni^{7+}	−45.120	6.5776	−3.7001	1.347 9	−0.447 22	0.108 59	−0.004 83	−0.003 67	0.000 98
Ni^{8+}	−46.639	7.3010	−3.8244	1.288 2	−0.309 73	−0.019 24	0.063 15	−0.037 05	0.014 48

with $E_{min} = 10$ eV and $E_{max} = 3000$ eV for this calculation. Note that the rate coefficient is the exponential of the standard Chebyshev polynomial expansion. The first eight Chebyshev polynomials are

$$\begin{aligned} T_1(x) &= x \\ T_2(x) &= 2x^2 - 1 \\ T_3(x) &= 4x^3 - 3x \\ T_4(x) &= 8x^4 - 8x^2 + 1 \\ T_5(x) &= 16x^5 - 20x^3 + 5x \\ T_6(x) &= 32x^6 - 48x^4 + 18x^2 - 1 \\ T_7(x) &= 64x^7 - 112x^5 + 56x^3 - 7x \\ T_8(x) &= 128x^8 - 256x^6 + 160x^4 - 32x^2 + 1. \end{aligned} \tag{8}$$

A computationally faster method of evaluating Chebyshev polynomials has been devised by Clenshaw (1955), and a sample program based on Clenshaw's algorithm is available (Pindzola *et al* 1987).

5. Summary and conclusions

Cross sections for ionisation of Ni^{5+}, Ni^{6+}, Ni^{7+}, Ni^{8+}, Ni^{12+} and Ni^{14+} have been measured, and ionisation rate coefficients have been calculated based on the data for Ni^{5+}-Ni^{8+}. Comparisons between the experimental data and distorted-wave calculations show that indirect ionisation processes contribute 30-50% of the peak total cross section for these nickel ions. Excitation of inner-subshell electrons to numerous autoionising levels contributes to a featureless enhancement of the cross sections for Ni^{5+}-Ni^{8+}. The $\Delta n = 1$ 2p-3p and 2p-3d transitions dominate excitation-autoionisation in Ni^{12+} and Ni^{14+} and play an important role in electron impact ionisation for these ions. This work greatly extends the range of available data for the nickel isonuclear sequence and provides a basis for comparison with future detailed calculations or studies of cross section scaling laws.

Acknowledgments

The authors acknowledge valuable assistance from and discussions with R A Phaneuf, D C Griffin, M J Buie and M S Pindzola during this project. Permission to use and

discuss calculated cross sections prior to publication is especially noted. Technical assistance from H T Hunter and J W Hale is also acknowledged. The production of nickel ion beams was made possible by help from F W Meyer. This work was supported by the Office of Fusion Energy, US Department of Energy, under contract No DE-AC05-840R21400 with Martin Marietta Energy Systems, Inc.

References

Abramowitz M and Stegun I A 1970 *Handbook of Mathematical Functions* (New York: Dover) p 795
Barnett C F 1983 *Nucl. Instrum. Methods* **214** 1
Belic D S, Falk R A, Dunn G H, Gregory D C, Cisneros C and Crandall D H 1981 *Bull. Am. Phys. Soc.* **27** 49
Buie M J and Pindzola M S 1987 Private communication
Burgess A and Chidichimo M A 1983 *Mon. Not. R. Astron. Soc.* **203** 1269
Burke P G, Fon W C and Kingston A E 1987 *J. Phys. B: At. Mol. Phys.* **20** 2579
Clenshaw C W 1955 *Math. Tables Other Aids Comput.* **9** 118
Cowan R D 1981 *The Theory of Atomic Structure and Spectra* (Berkeley: California University Press)
Cox M G and Hayes J G 1973 *United Kingdom National Physical Laboratory Report No NAC 26*
Crandall D H and Phaneuf R A 1978 *Phys. Rev.* A **18** 1911
Gregory D C and Howald A M 1986 *Phys. Rev.* A **34** 97
Gregory D C, Meyer F W, Muller A and Defrance P 1986 *Phys. Rev.* A **34** 3657
Gregory D C, Wang L J, Meyer F W and Rinn K 1987 *Phys. Rev.* A **35** 3256
Isler R C 1984 *Nucl. Fusion* **24** 1599
Isler R C, Neidigh R V and Cowan R D 1977 *Phys. Lett.* **63A** 295
Lotz W 1968 *Z. Phys.* **216** 241
Mathews J and Walker R L 1970 *Mathematical Methods of Physics* (New York: Benjamin Cummings)
Meyer F W 1985 *Nucl. Instrum. Methods* **9** 532
Montague R G, Diserens M J and Harrison M F A 1984 *J. Phys. B: At. Mol. Phys.* **17** 2085
Montague R G and Harrison M F A 1985 *J. Phys. B: At. Mol. Phys.* **18** 1419
Mueller D W, Morgan T J, Dunn G H, Gregory D C and Crandall D H 1985 *Phys. Rev.* A **31** 2905
Palumbo D 1971 *Phys. Scr.* **23** 69
Pindzola M S, Griffin D C, Bottcher C, Gregory D C, Howald A M, Phaneuf R A, Crandall D H, Dunn G H, Mueller D W and Morgan T J 1985 *Oak Ridge National Laboratory Report No ORNL/TM-9436*
Pindzola M S and Griffin D C 1987 Private communication
Pindzola M S, Griffin D C and Bottcher C 1983 *J. Phys. B: At. Mol. Phys.* **16** L355
—— 1986 *Phys. Rev.* A **34** 3668
Pindzola M S, Griffin D C, Bottcher C, Younger S M and Hunter H T 1987 *Oak Ridge National Laboratory Report No ORNL/TM-10297*
Taylor P O, Dolder K T, Kauppila W E and Dunn G H 1974 *Rev. Sci. Instrum.* **45** 538